# Detonation Wave Propagation
# and Interaction
# with Transportation Infrastructure

by

K. M. Isaac, P. Shivaram, W. P. Schonberg, and C. Renfro

UTC
R170

## *Disclaimer*

The contents of this report reflect the views of the author(s), who are responsible for the facts and the accuracy of information presented herein. This document is disseminated under the sponsorship of the Department of Transportation, University Transportation Centers Program and the Center for Infrastructure Engineering Studies UTC program at the University of Missouri - Rolla, in the interest of information exchange. The U.S. Government and Center for Infrastructure Engineering Studies assumes no liability for the contents or use thereof.

**Technical Report Documentation Page**

| 1. Report No.<br><br>UTC R170 | | 2. Government Accession No. | 3. Recipient's Catalog No. |
|---|---|---|---|
| 4. Title and Subtitle<br><br>Detonation Wave Propagation and Interaction with Transportation Infrastructure | | | 5. Report Date<br><br>January 2008 |
| | | | 6. Performing Organization Code |
| 7. Author/s<br><br>K. M. Isaac, P. Shivaram, W. P. Schonberg, and C. Renfro | | | 8. Performing Organization Report No.<br><br>00013063 |
| 9. Performing Organization Name and Address<br><br>Center for Infrastructure Engineering Studies/UTC program<br>Missouri University of Science & Technology<br>223 Engineering Research Lab<br>Rolla, MO 65409 | | | 10. Work Unit No. (TRAIS) |
| | | | 11. Contract or Grant No.<br><br>DTRS98-G-0021 |
| 12. Sponsoring Organization Name and Address<br><br>U.S. Department of Transportation<br>Research and Special Programs Administration<br>400 7th Street, SW<br>Washington, DC 20590-0001 | | | 13. Type of Report and Period Covered<br><br>Final |
| | | | 14. Sponsoring Agency Code |
| 15. Supplementary Notes | | | |

16. Abstract

The recent establishment of the National University Transportation Center at MST under the "Safe, Accountable, Flexible, Efficient Transportation Equity Act: A Legacy for Users," expands the research and education activities to include alternative transportation fuels and other issues that are at the forefront of society and the national agenda. MST in partnership with MTI will establish a rural hydrogen transportation test bed for developing, demonstrating, evaluating, and promoting hydrogen-based technologies in a real-world environment. The State of Missouri is ideally suited to develop and demonstrate the proper operation of hydrogen highways in a rural setting, which represents over 25 percent of the nation's transportation needs and which is not well-represented in the current major national projects. A holistic approach will be taken to address not just the technology but also public perception, permitting, safety standards, and education and training. A key partner already engaged is the NASFM, who regards this project as an "excellent candidate for the model approach to introducing hydrogen to communities." The tasks identified in five areas, viz., Infrastructure Development and Deployment, High-Pressure Composite Cylinders, Inspection and Monitoring, Statistically Validated Codes and Standards, and Safety, constitute a comprehensive research, development and demonstration program to address some of the challenges described in the U.S. Department of Transportation Hydrogen Roadmap 2005.

| 17. Key Words<br><br>Hydrogen Transportation Systems, Composite Storage Tanks, Infrastructure Development and Deployment, Non-Destructive Testing and Evaluation, Safety Codes and Standards, Safety Education, Outreach and Training | | 18. Distribution Statement<br><br>No restrictions. This document is available to the public through the National Technical Information Service, Springfield, Virginia 22161. | | |
|---|---|---|---|---|
| 19. Security Classification (of this report)<br><br>unclassified | | 20. Security Classification (of this page)<br><br>unclassified | 21. No. Of Pages<br><br>7 | 22. Price |

Form DOT F 1700.7 (8-72)

# Detonation Wave Propagation and Interaction with Transportation Infrastructure

K. M. Isaac,[1] P. Shivaram,[2] W. P. Schonberg,[3] and C. Renfro[4]
*University of Missouri-Rolla, Rolla, MO 65409*

**Propagation of the blast wave caused by hydrogen-air detonation, and the blast wave interaction with a transportation infrastructure are studied. A cylindrical blast wave and a planar blast wave are investigated. RHT-35MPA concrete is the material used for a wall to model the interaction. The blast wave-structure interaction shows that the structure can fail in different modes depending on the material properties. Concrete has failure features quite distinct from metals such as steel and aluminum.**

## I.  Introduction

$H$YDROGEN has emerged as a prime candidate as an alternative fuel in the strategy to reduce dependence on fossil fuels. Hydrogen has advantages over hydrocarbon fuels because it doesn't produce greenhouse gases such as $CO_2$. Hydrogen can be produced from a wide range of feedstock such as natural gas, ethanol and brewery byproducts. While the economics are being debated, it is generally accepted that hydrogen is cost-competitive if factors such as global warming are included in the cost considerations. Associated with the increasing use of hydrogen are several issues that must be addressed. Safety is one such important issue. Safety considerations must be included in the planning and implementation of the hydrogen transportation infrastructure. Hydrogen for transportation use may take different forms depending on the technology being considered. These form include gaseous, liquid, slush, and hydrides. The hazard issues associated with each form must be assessed for a systematic evaluation of the various technologies. Gaseous hydrogen is much lighter than air, highly diffusive, conducive to flow-induced static charge generation, leak-prone, colorless and odorless. As it is a very light gas, it requires high pressure storage (5000-10,000 psi). High pressure rupture and flying debris are of greater concern. Pipe whip caused by leak events, oxygen displacement in confined spaces, and gas jet impingement damage can occur in accidents involving stored hydrogen. Hydrogen is flammable with no luminous flame and no toxic combustion products. It has a large flammability range—4%-74% by volume—and can deflagrate at low pressures and detonate at high pressures. It also has low ignition energy—0.02 mJ-1mJ spark to ignite a deflagration—and has a modest autoignition temperature of ~575$^o$C. Metals and plastics are prone to hydrogen embrittlement posing challenges to storage and piping. Boiloff losses from liquid hydrogen storage tanks are large and the gas quickly diffuses into the surroundings creating hazardous situations. Flow-induced static charge generation is high. Rapid phase change from liquid to vapor can lead to explosive pressure levels. Condensing gases from air contact cause easy contamination. Colorization and odorization to improve detection are difficult because additives freeze at cryogenic storage temperatures. Cryogenic burns, especially eyes, lung damage from cold vapor inhalation, and hypothermia are possible health hazards. Air condensation can result in oxygen-rich environment which may create favorable ignition scenarios. High thermal gradients from cryogenic to ambient temperature induce high thermal stresses on storage system components. Materials have low specific heats at low temperatures which reduce the time lag of events that follow an explosion. The safety aspects of slush hydrogen are very similar to those of liquid hydrogen. It can plug passageways and suddenly build up pressure. Slush can also be contaminated by condensing gases. There are additional flammability concerns associated with organic hydrides. Some have low autoignition temperatures. And some are also toxic. The main advantage of hydrides is that the operating pressures are low. However, hydrogen decomposition may require temperatures close to $H_2$ autoignition temperature. The organics released during thermal decomposition may have health effects as well as the potential to foul components of the power

---

[1] Professor, Mechanical & Aerospace Engineering, 102 ME Building, Associate Fellow.
[2] Graduate Assistant, Mechanical & Aerospace Engineering.
[3] Professor, Civil, Environmental & Architectural Engineering, Associate Fellow.
[4] Undergraduate Assistant, Mechanical & Aerospace Engineering, Student Member.

system. Temperatures as high as 400°C are needed to evolve $H_2$ from the liquid organic hydrides. The hot gas can cause thermal burns. The vehicles electrical power source (12V battery) can be used for heating; however, it also is another source of ignition. Some metals used in metal hydrides are pyrophoric/flammable; some may also be toxic. The operating pressures of metal hydride systems are similar to those of liquid organic hydrides. Hydride formation is exothermic causing heat release during loading. Release temperatures are similar to liquid organic hydrides, and the safety issues related to heating the hydride are also similar. Metal oxidation is to be considered in design and operation. Some metals have threshold limit values (TLV) for long term occupational exposure. Recent efforts to use hydrides include using carbon nano tubes (CNT). Many of the safety issues of CNTs are similar to those of other hydrides. However, ongoing research may uncover additional safety concerns in using CNTs.

## II. Previous Work

A common approach is to model an explosion as an ideal spherical blast wave with a pressure profile approximated by an analytic function scaled according to empirical laws. The spherical blast wave propagates without distortion, and the pressure jump across the wave loads structures in its path causing the structure to respond. The structure can be modeled with varying degrees of complexity. Another approach used in the motion picture industry emphasizes the visual effects more than the physics. In many previous studies the detonation that causes the blast wave are not modeled. Instead initial conditions for the simulations are assumed based on the rudimentary models of the energy released in a detonation.

In the present work we use a detailed model for the detonation that takes into account finite-rate chemical reactions involving multiple species and reaction steps[1,2]. The wave properties thus obtained are used as the initial conditions for modeling the blast wave, thus providing more accurate wave characteristics.

Figure 1 shows the diagram of a stationary detonation wave. Fuel-air mixture flows from the left at the detonation wave Mach number. The coordinate system is fixed to the wave. The mixture is auto-ignited at some point downstream and the flow accelerates to Mach number = 1 under Chapman-Jouguet (CJ) conditions. By neglecting wall effects, the equations
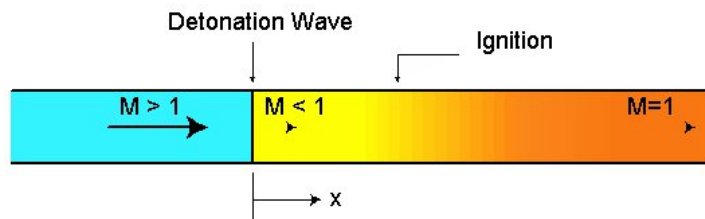


**Figure 1. Detonation wave structure (Griner and Isaac[1] and Isaac and Scott[2])**

governing the steady wave process can be written in the one-dimensional form with streamwise coordinate x as the independent variable. The governing conservation equations form a set of coupled ordinary differential equations for mass, momentum, energy and chemical species. These equations are supplemented by equations to calculate thermodynamic properties of the individual species and the gas mixture. Further details can be found in Refs. 1 and 2. The set of equations can be solved by a suitable integration scheme that can handle the "stiffness" caused by the species production terms present in the equations. The species production rate for each species must be calculated using the rate constants of each of the reactions considered. Chemkin II routines[3] have been used for calculating chemical kinetics and thermodynamic properties at each integration step. The integration step size was typically $10^{-4}$ cm.

Chao and Shepherd,[4-6] Baum et al,[7] and Oran et al.[8] have studied blast wave interaction with structures. The present work is based on numerical simulations of blast wave structure interaction using the software package AUTODYN.[9] It has been used for many impact, penetration and explosion studies and found to yield reliable results.

**Solver Overview**

The various numerical processors available in AUTODYN generally use a coupled finite difference/finite volume approach.[10] This scheme allows a choice of numerical processors to be selectively used to model different regimes/components of the problem. The respective structured meshes are operated on by the appropriate processors coupled in space and time to solve problems involving fluids and structures that interact with each other. The numerical processors include: the Lagrange processor for modeling solid continua and structures, Euler processor for modeling liquids, gases and large distortion solids, ALE (arbitrary Lagrange Euler) for specialized flow models, shell processor for modeling thin walled structures, and SPH (smooth particle dynamics) for specialized problems.

SPH has features similar to meshless solvers. It is a Lagrangian method that models regions only where material exists. It tracks material interfaces fairly accurately. It can handle complex constitutive models. All the above processors use explicit time integration, and therefore AUTODYN is well suited for dynamic phenomena over short periods such as impacts and explosions. Viscous effects are not modeled.

The Lagrange processor operates on a structured (I-J-K) mesh of quadrilateral or hexahedral cells. The vertices of the mesh move with material flow velocity. Material in each cell remains the same with no cell-to-cell material transport. Because there is no calculation of material transport, the method tends to be faster compared to the Euler method. Material interfaces, free surfaces and material behavior history are easy to follow in the Lagrange formulation. The method has a major disadvantage that if large material movement occurs, the mesh will become highly distorted leading to inaccurate and inefficient solution, ultimately leading to termination of the calculation. Remapping the solution on to a regular mesh is a procedure used in AUTODYN to alleviate the mesh distortion problem.
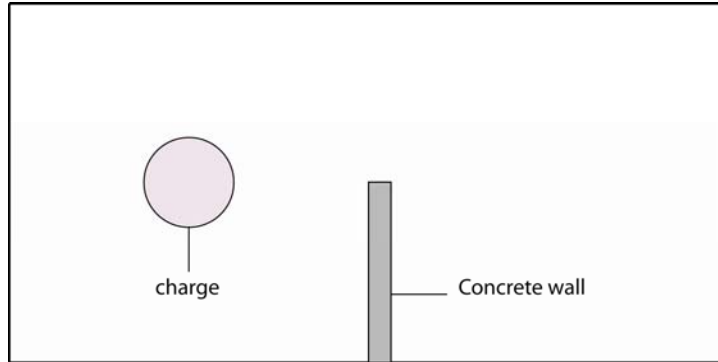


**Figure 2.  8 m x 4 m solution domain. 2 m x 0.3 m concrete wall is placed midway in the rectangular region. 1 m diameter high pressure, high temperature gas region is 2m each from the left and bottom walls.**

In addition to the original first order scheme, two higher order Euler schemes are also available. The Godunov multimaterial with strength higher order and the FCT higher order[11-13] single material are the available higher order schemes. A control volume formulation is used for the conservation equations in the Euler schemes. Terms producing changes in conserved variables are divided into two groups: Lagrangian or convective. A two-step method is used to advance the solution to the next time level. In the first Lagrangian step, the Lagrangian variables are advanced to the next time level. In the next Euler step, the updated variables are mapped on to the Euler mesh. All variables are cell-centered, facilitating arbitrary shaped control volumes to be formed at the interface between the Lagrange and Euler meshes. This allows greater flexibility in solving fluid-structure interaction problems.

Coupling of separate numerical grids across Lagrange-Lagrange and Euler-Lagrange interfaces are permissible. There are four different types of coupling used. Joined Lagrange grids has node-to-node contact, which move according to the stress distribution in all the surrounding elements. Joined Euler grids also allow node-to-node



**Figure 3. Pressure contours at 305 microseconds.**

type of contact. In Joined Euler grids, material can flow from one mesh to another. Impact/slide interfaces allow Lagrange grid to impact/slide along any Lagrange interface. This surface can be dynamically redefined as the surface changes through erosion, a technique wherein Lagrange cells are transformed into free mass points not connected to the original mesh. These eroded elements can further interact with other bodies. Euler-Lagrange
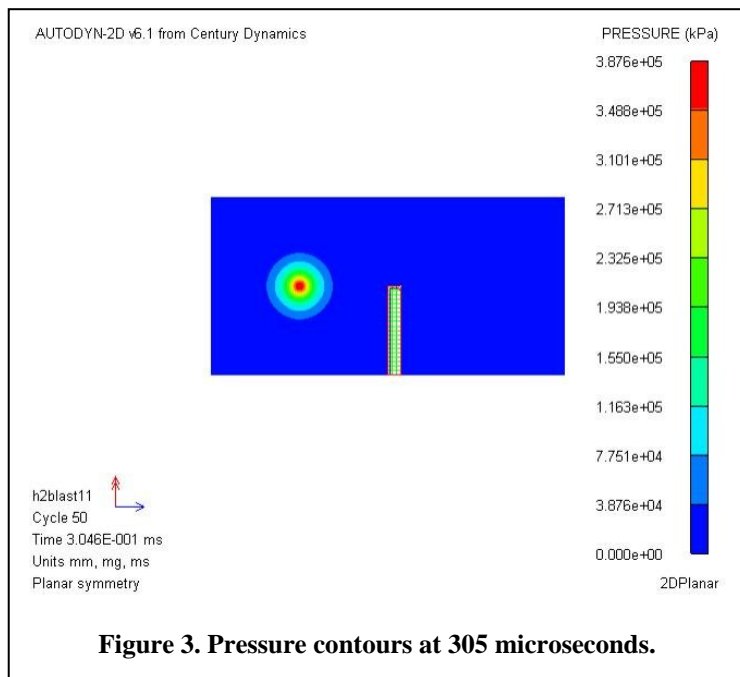
coupling is implemented in a very general way. The Lagrange mesh may cut through a fixed Euler grid. The intersected Euler cells define a stress profile for the Lagrange boundary vertices, whereas the Lagrange interface define a geometric constraint to the flow of material in the Euler mesh. To avoid small cell volumes during the interaction, merging of small Euler cells into larger cells is done dynamically. The reverse process of splitting of
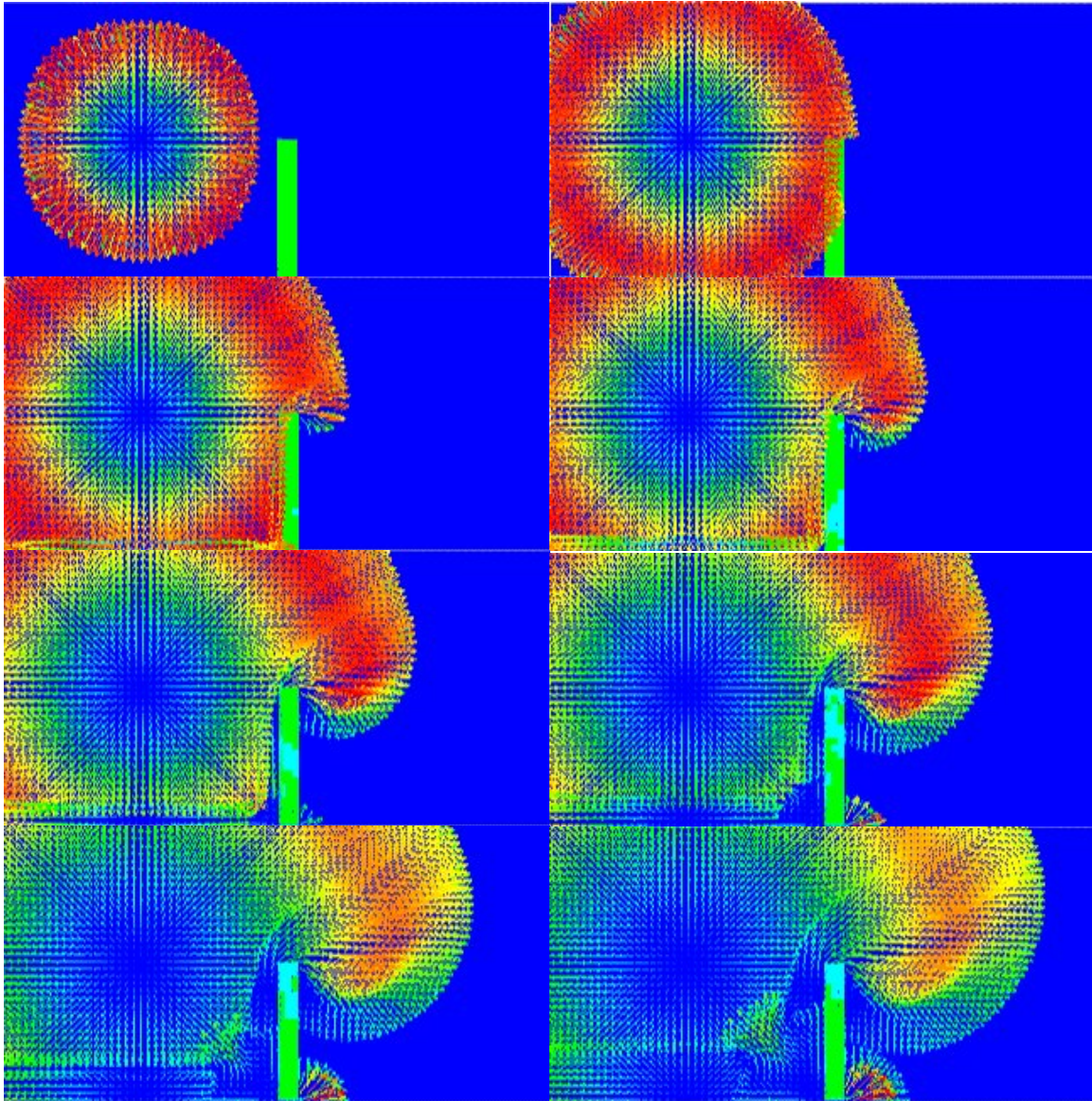


**Figure 4. Velocity vectors at 8 instants. Left column top to bottom: Frames 1, 3, 5 and 7. Right column top to bottom: Frames 2, 4, 6 and 8.**

large cells into smaller ones is also done.

Materials with very general equations of state can be modeled. Yield models include constant (von Mises), piecewise linear, Mohr-Coulomb work hardening, and a number of strain hardening and thermal softening models. Orthotropic yield behavior and failure criteria may also be defined.

In this work we set up a few cases to study the effect of a cylindrical volume of hydrogen-air detonating and the resulting blast wave interacting with a concrete wall. The objective of the study is to determine if the structure can withstand the blast wave. The blast wave was created by detonating a stoichiometric hydrogen-air mixture contained

in a 1 m diameter cylindrical region, at a pressure ~340 atm (5000 psi) and 300K temperature. This pressure is representative of the expected pressure levels for hydrogen storage at refueling stations. The detonated gas properties were obtained using a constant-volume equilibrium calculation.
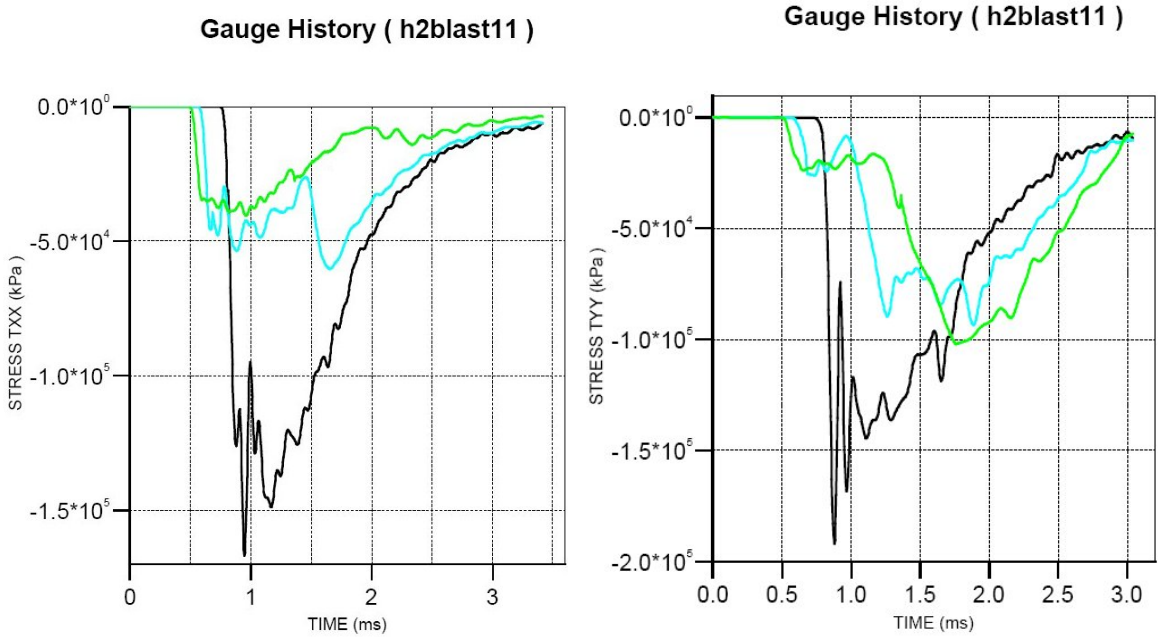
**Gauge History ( h2blast11 )**

**Gauge History ( h2blast11 )**

**Figure 5. Stress history for gage points 1, 2 and 3. Black: Gage 1, Blue: Gage 2, Green Gage 3.**

**Gauge History ( h2blast15 )**

**Gauge History ( h2blast15 )**

**Figure 6. Stress history for gage points 1, 2 and 3. Black: Gage 1, Blue: Gage 2, Green: Gage 3.**

American Institute of Aeronautics and Astronautics

The concrete wall is 0.3 m thick and 2 m high. A partial list of the concrete material properties are as follows[14]: Equation of State: P-alpha, Porous density: 2.31400E+00 (g/cm$^3$), Initial compaction pressure: 2.33000E+04 (kPa), Solid compaction pressure: 6.00000E+06 (kPa), Compaction exponent: 3.00000E+00 (none), Solid EOS: Polynomial, Bulk Modulus: A1 3.52700E+07 (kPa), Parameter A2: 3.95800E+07 (kPa), Parameter A3: 9.04000E+06 (kPa), Parameter B0: 1.22000E+00 (none), Parameter B1: 1.22000E+00 (none), Parameter T1: 3.52700E+07 (kPa), Parameter T2: 0.00000E+00 (kPa ), Compaction Curve: Standard, Strength model: RHT Concrete, Shear Modulus: 1.67000E+07 (kPa ), Compressive Strength: (fc) 3.50000E+04 (kPa), Tensile Strength: (ft/fc) 1.00000E-01 (none), Shear Strength: (fs/fc) 1.80000E-01 (none), Intact Failure Surface Constant A: 1.60000E+00 (none), Intact Failure Surface Exponent N: 6.10000E-01 (none), Tens./Comp. Meridian Ratio (Q): 6.80500E-01 (none), Brittle to Ductile Transition: 1.05000E-02 (none), G (elas.)/(elas.-plas.): 2.00000E+00 (none), Elastic Strength/ft: 7.00000E-01 (none), Elastic Strength/fc: 5.30000E-01 (none), Fractured Strength Constant B: 1.60000E+00(none), Fractured Strength Exponent M: 6.10000E-01 (none), Compressive Strain Rate Exp. Alpha: 3.20000E-02 (none), Tensile Strain Rate Exp. Delta: 3.60000E-02 (none), Max. Fracture Strength Ratio: 1.00000E+20 (none), Use CAP on Elastic Surface?: Yes, Failure model: RHT Concrete, Damage Constant, D1: 4.00000E-02 (none), Damage Constant, D2: 1.00000E+00 (none), Minimum Strain to Failure: 1.00000E-02 (none), Residual Shear Modulus Fraction: 1.30000E-01 (none), Tensile Failure: Principal Stress, Principal Tensile Failure Stress: 5.00000E+03 (kPa), Max. Princ. Stress Difference/2: 1.01000E+20 (kPa), Crack Softening: Yes, Fracture Energy: Gf (=[K$^2$]/E), 1.00000E+02 (J/m$^2$ ), Flow Rule: No Bulking, Stochastic failure: No, Erosion: Geometric Strain, Erosion Strain: 2.00000E+00 (none), Type of Geometric Strain: Instantaneous.

## III.  Results and Discussion

The 8 frames Fig. 4 are ordered in the document reading format. In the left column, top to bottom, are frames 1,3,5, and 7, and in the right column, top to bottom, are frames 2, 4, 6 and 8. Frame 1 is at 305 micro s after initiation. The last frame is at 1.82 ms from the start. Since time integration uses adaptive time-stepping, the time interval between consecutive frames is not constant. The frames show velocity vectors colored by magnitude. The progressing blast wave front can be clearly seen in the frames. As the wave impacts the wall, the high pressure causes the concrete to be highly stressed and parts of it reach plastic deformation state. The changing color indicates material status. Slight erosion is present in the later frames. Another indication of the concrete wall failure is the gas leaking from left to right at the base of the wall. The concrete begins to fail at about 800 micro s from the start.

Figure 5 shows stresses $\tau_{xx}$ and $\tau_{yy}$ at three different locations (gage points) on the concrete wall. These gage points are designated by their I-J indices as: (2,2), (2,11), and (2,20). These are I-J indices for the wall starting with I = 1 for left face and J = 1 for the bottom edge. For the wall, I ranges 1-4 and J ranges 1-21. (The region enclosing the wall has its own I-J indices.) Figure 5, $\tau_{xx}$(left), shows that the top-most gage point is stressed first, followed by the middle gage point, and then the bottom-most gage point. As expected all the three gage points are in compression (stress values are negative). It is interesting to note that this compressive stress is the highest at the base and lowest at the top. The maximum stress (~ -1.5e5 kPa) at the base is reached in about 1 ms. The stress curves at the middle and top gage points are flatter and the maxima are much smaller than that at the base. In about 3 ms, the stress values at all the three gage locations return to near zero. The $\tau_{yy}$ history (right) in Fig. 5 is similar to the $\tau_{xx}$ history. The values at gage locations 2 and 3 are slightly higher.

Figure 6 shows results from a planar blast wave impacting the concrete wall. The wave travels at 1000 m/s, density = 0.1 g/cc, and pressure = 4000 kPa. Significant differences in the stress histories for Gages 1, 2 and 3 from the previous case of the cylindrical blast wave are apparent. These differences can be attributed mainly to the differences in the pressure variation along the wall. The planar wave is seen to create a larger pressure at the base than at the top as the wave traverses the wall. There are also differences in the displacement pattern after the wall fails and starts moving.

## IV.  Conclusion

Numerical simulations of blast waves interacting with a solid concrete wall discussed in this work provide many insights into the nature of the concrete wall response and the failure modes. These results are directly applicable to assessing safety issues related to using hydrogen for transportation. Even at a storage pressure of about 5000 psi (the

lower end of the expected pressure range), damage is catastrophic. Thicker walls and stronger concrete material may help reduce the severity of the explosion. Failure is complete within about 3 ms from the start of the explosive event. The results presented are preliminary, and large number of simulations are necessary to draw more broader conclusions and develop codes and standards for transportation infrastructure for hydrogen-fueled vehicles. More realistic structures and storage containers need to be included in the simulations. These aspects will be addressed in future studies.

## Acknowledgments

## References

[1]Griner, J. and Isaac, K. M., "Induction Time and Detonation Wave Structure of Acetylene, Ethylene and JP-10," Central States Section of the Combustion Institute, Spring 2002 Meeting, April 2002.

[2]Isaac, K. M. and Scott, T., "Ignition Delay and Detonation Wave Structure using Detailed Chemical Kinetics Mechanisms," 2nd Joint Meeting of the US Sections of the Combustion Institute, March 2001.

[3]Kee, R. J., Rupley, F. M., and Miller, J. A., Chemkin-II: A Fortran Chemical Kinetics Package for the Analysis of Gas-Phase Chemical Kinetics, Sandia National Laboratories Report SAND89-8009, 1989.

[4]Chao, T. –W. and Shepherd, J. E., "Fracture Response of Externally-Flawed Cylindrical Shells to Internal Gaseous Detonation Loading," Emerging technologies in Fluids, Structures, and Fluid-Structure Interactions, PVP Vol. 462-2, 85-98, 2002.

[5] Chao, T. –W. and Shepherd, J. E., "Comparison of fracture response of preflawed tubes under internal static and detonation loading," Journal of Pressure Vessel Technology, 126(3):345-353, August 2004.

[6] Chao, T. –W. and Shepherd, J. E., "Fracture response of externally flawed aluminum cylindrical shells under internal gaseous detonation loading," International Journal of Fracture, 134(1):59-90, July 2005.

[7]Baum, J. D., Mestreau, E. L., Luo, H., and Lohner, R., "Modeling of Near-Field Blast Wave Evolution," AIAA 2006-191, 44th AIAA Aerospace Sciences Meeting, 2006.

[8]Oran, E. S., (private communication, 2006)

[9]AUTODYN User Manual, Version 6.1, Century Dynamics, Inc., 2003.

[10]Cowler, M. S. and Hancock, S. L. "Dynamic fluid-structure analysis of shells using the PISCES 2 DELK computer code," Proceedings of the Fifth International Conference on Applied Mechanics, 1979.

[11]Boris, J. P.; Book, D. L. "Solution of continuity equations by the method of flux-corrected transport," Naval Research Laboratory Report, Washington, D.C., pp. 85-129, 1976.

[12]DeVore, C. R. and Oran, E. S., "The stability of imploding detonations in the geometrical shock dynamics (CCW) model," Physics of Fluids A: Fluid Dynamics, April 1992, Volume 4, Issue 4, pp. 835-844.

[13]Liua, J., Oran, E. S. and Kaplan, C. R., "Numerical diffusion in the FCT algorithm, revisited," Journal of Computational Physics, Volume 208, Issue 2 , 20 September 2005, Pages 416-434.

[14]Riedel, W., "Beton unter dynamischen Lasten," Ph. D. Thesis,  EMI, Freiburg. Germany, 2000.